J Solid State Eletrochem (2004) 8: 167–173
DOI 10.1007/s10008-003-0441-5

ORIGINAL PAPER

Yutaka Fujiwara · Hidehiko Enomoto

# Intermetallic phase formation in electrochemical alloy deposition

Received: 10 December 2002 / Accepted: 10 March 2003 / Published online: 27 September 2003


**Abstract** Three examples of the electrochemical deposition of intermetallic phases are shown. Electrodeposition of the single-phase $\beta'$-brass superlattice at underpotentials of Zn in Cu-Zn alloy plating is explained by an accumulative underpotential deposition (UPD) mechanism. Growth of the Cu-Sn intermetallic phase layer in the contact immersion deposition of Sn onto Cu is accounted for by a UPD/vertical solid-state diffusion mechanism. $Ag_3Sn$ formation in the Sn/Ag-nanoparticle composite plating is illustrated by atomic site exchange at the interface between the deposited Sn matrix and the occluded Ag nanoparticles.

**Keywords** Electrochemical deposition · Intermetallic phases · Site exchange · Solid-state diffusion · Underpotential deposition

## Introduction

Electrochemically deposited alloy films have a wide range of applications, from microelectronic devices to the corrosion protection of steel sheets. Brenner [1] first described the abnormal behavior of alloy deposition in terms of the deposit composition. Brenner's "abnormal" codeposition includes two different types of behavior: "anomalous" and "induced" codeposition. Anomalous codeposition signifies that the less noble component of the alloy deposits preferentially. Induced codeposition indicates that a metal that cannot be deposited, such as W or Mo, is deposited as a component of alloys.

Y. Fujiwara (✉) · H. Enomoto
Osaka Municipal Technical Research Institute,
1-6-50 Morinomiya, Joto-ku,
536-8553 Osaka , Japan
E-mail: fujiwara@omtri.city.osaka.jp
Tel.: +81-6-69638087
Fax: +81-6-69638099

Abnormal types of behavior concerning the deposit structure have also been observed; these include the formation of a metastable intermetallic phase such as NiSn [2] and the deposition of amorphous Ni-P alloys [3].

These types of behavior imply that the alloy deposition processes are normal, although the deposited alloy films have an abnormal composition and/or structure in view of the thermodynamic considerations. In addition, most of these films are deposited at overpotentials, that is, at potentials more negative than the reversible potential of the individual components.

On the other hand, electrochemical deposition of thermodynamically stable intermetallic phases through peculiar processes is occasionally observed in practical alloy deposition systems. A peculiar process includes alloy deposition at underpotentials of the less noble component. A typical example is the electrodeposition of single-phase CdTe [4, 5]. In this case, the underpotential deposition (UPD) of the less noble component, Cd, proceeds simultaneously with diffusion-limited Te deposition. The UPD generally means the deposition of a submonolayer or monolayer of a foreign metal adatom onto a surface. However, the bulk alloys consisting of the deposited metal and the substrate metal can be formed in the UPD range if they can form solid solutions [6] or intermetallic phases [7]. In the case of CdTe deposition, the deposited Te atoms act as the "substrate" for the UPD of Cd atoms. Horkans et al. [8] pointed out the important role of the UPD phenomenon in alloy deposition.

This paper describes three cases of electrochemical deposition of thermodynamically stable intermetallic phases in practically important processes. The deposition mechanisms of these phases are discussed and their peculiarities are shown.

First, it is shown that the single-phase $\beta'$-brass superlattice films are electrodeposited at underpotentials of Zn. Cu-Zn alloy (brass) plating is important practically as a decorative finishing [9, 10]. Second, Cu-Sn intermetallic phase formation in a contact immersion

deposition of Sn onto Cu is described. The role of Sn UPD and the "vertical" solid-state diffusion is discussed. Immersion Sn deposition onto Cu is used as a solderable coating in printed wiring board fabrication. Finally, the structure of electrodeposited Sn-Ag alloy films is shown. Although the films are deposited via the Sn/Ag-nanoparticle composite plating, $\beta$-Sn and $Ag_3Sn$ are obtained. Electrodeposited Sn-Ag alloy films are applied to the solderable coatings for Pb-free solder bonding [11].

## Experimental

All the deposition solutions were prepared using reagent grade chemicals and water purified by a Millipore Milli-RX12 Plus system.

X-ray diffraction (XRD) pattern measurements were performed using a MAC Science Model MXP-18 X-ray diffractometer system and monochromated Cu K$\alpha$ radiation to identify the deposited phases.

### Electrodeposition of $\beta'$-brass from cyanide solutions

Cu-Zn alloys were electrodeposited under potentiostatic conditions from solutions containing 0.30 M CuCN, 0.05, 0.10 or 0.30 M $Zn(CN)_2$ and NaCN at 25 °C in a $N_2$ atmosphere without stirring. NaCN concentrations of the solutions were 0.90, 1.00 or 1.40 M, respectively. A Zn solution containing 0.100 M $Zn(CN)_2$ and 0.237 M NaCN was also used for separate Zn deposition experiments. The NaCN concentrations were defined so that the free $CN^-$ concentration was equal in all solutions [12], by considering the stability constants of the cyanide complexes [13].

The cathode was a Cu-plated Pt sheet for determining the alloy composition and the partial current density in the alloy deposition, and was a Cu-plated mild steel sheet for the XRD measurements. The counter electrode was a Pt-coated Ti sheet, and the reference electrode was a Ag/AgCl electrode in a saturated KCl solution. All the electrode potentials are referred to the Ag/AgCl (in saturated KCl) electrode in this paper.

A Seiko model SPS 1500VR inductively coupled plasma–atomic emission spectrometer (ICP-AES) was used to determine the compositions of the deposited films. The partial current densities of Zn deposition were also determined from ICP-AES concentration measurements using Faraday's law. The partial currents of Zn deposition and dissolution in the $Zn^{2+}$ cyanide solution were estimated from the weight change of the Zn electrode.

### Contact immersion deposition of Sn

Sn(II)–citrate solutions containing 0.1 M $SnSO_4$ and 1.0 M trisodium citrate (pH 6.2) were used for the contact immersion Sn deposition. Two series of deposition experiments were carried out in a $N_2$ atmosphere. First, a Cu substrate was dipped in suspensions of 90 g/dm$^3$ metallic Sn powder (diameters below 150 μm) in the Sn(II)–citrate solution. Second, a Cu substrate and a Sn sheet were dipped in the Sn(II)–citrate solution without the suspended Sn powder and were allowed to contact each other electrically outside the solution. The solutions were vigorously agitated with a magnetic stirrer.

The amount of deposited Sn was determined by ICP-AES analysis. The immersion potentials of a Cu substrate and a Sn sheet in the Sn(II)–citrate solution were measured against a Ag/AgCl (in saturated KCl) electrode.

### Sn/Ag-nanoparticle composite plating

The solution for the deposition of Sn-Ag alloys contained 0.1 M $SnSO_4$, 0.2 M $K_4P_2O_7$, 0.01 M $AgNO_3$ and 1 g/L poly(ethylene glycol) 6000 (pH 8.0). The color of the solutions containing $SnSO_4$, $K_4P_2O_7$ and $AgNO_3$ was black, although both the $SnSO_4/K_4P_2O_7$ and $AgNO_3$ solutions were transparent. To confirm that the black solutions are the suspensions of fine particles, dialysis experiments were carried out using a cellulose tube with a nominal pore size of 2.4 nm.

Electrodeposition runs were performed at 50 °C and at 10 mA/cm$^2$ and with mild stirring using a magnetic stirrer. The cathode was a Cu sheet and the anode was a Sn sheet.

The residue in the dialysis tube and the cross section of the electrodeposited Sn-Ag alloy films were examined by a JEOL JEM-1200EX transmission electron microscope (TEM). The sliced thin specimen of the cross section of the electrodeposited film was prepared by a Leica ULTRACUT UCT ultra microtome.

## Results and discussion

### Electrodeposition of an intermetallic phase through accumulative UPD: electrodeposition of single-phase $\beta'$-brass from cyanide solutions

Abnormal behavior of the Cu-Zn alloy deposition from cyanide baths is known, that is, the Zn content of the deposits goes through a maximum as a function of the current density or overpotential [12]. The cause of the abnormal behavior is not thoroughly understood, but we [14] recently showed that the maximum Zn content is related to the UPD of Zn and the formation of the $\beta'$-brass superlattice.

#### *Composition and structure of electrodeposited Cu-Zn alloy films*

Figure 1 shows the Zn content of the alloy films as a function of the applied potential. Although separate Zn

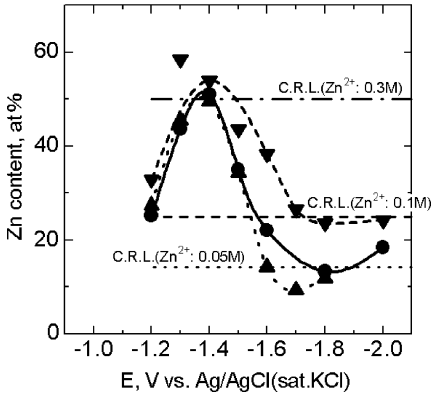


**Fig. 1** Zn content in the electrodeposited Cu-Zn alloy films from cyanide solutions as a function of the applied potential, *E*. Solution compositions: *up triangles*: 0.30 M CuCN, 0.05 M $Zn(CN)_2$, 0.90 M NaCN; *circles*: 0.30 M CuCN, 0.10 M $Zn(CN)_2$, 1.00 M NaCN; *down triangles*: 0.30 M CuCN, 0.30 M $Zn(CN)_2$, 1.40 M NaCN; C.R.L. represents the composition reference line where the composition of the electrodeposited alloy films are equal to the $Cu^+$ to $Zn^{2+}$ concentration ratio in the solutions

deposition occurred only at potentials more negative than −1.5 V, Zn was codeposited with Cu at more positive potentials as well, that is, in the UPD region. The Zn content of the alloy films showed a maximum near 50 at% at around −1.4 V, independent of the $Zn^{2+}$ concentration of the solutions.

Codeposition of Zn in the UPD region can clearly be seen from the partial current density–potential curves (*I–E* curves) of Zn deposition, shown in Fig. 2. The partial *I–E* curves of Zn in Cu-Zn alloy deposition were quite different from that of the separate Zn deposition from the solution without $Cu^{+}$ ions. Separate Zn deposition was observed only at potentials negative to −1.5 V, as noted above. Zn was dissolved in the $Zn^{2+}$ solution at potentials between −1.34 V and −1.5 V, although the total current was cathodic. On the other hand, Zn was deposited as Cu-Zn alloy films at −1.5 V and at more positive potentials from the $Cu^{+}$-containing solutions.

Figure 3 shows the XRD patterns of the alloy films electrodeposited at −1.4 V for which the compositions were near CuZn. All the diffraction peaks of the films were assigned to the intermetallic compound CuZn (JCPDS-ICDD 2-1231) [15]. The CuZn phase shows a reversible order–disorder transformation at around 460 °C, and the low-temperature ordered phase (the $\beta'$-brass), also called the superlattice, has a CsCl-type structure [15, 16, 17]. The superlattice is confirmed by the appearance of weak superlattice peaks in the XRD patterns, which vanish in the disordered structure [16]. A strong (111) superlattice peak was observed in the XRD patterns of the films from the low-$Zn^{2+}$ concentration solutions, although this was not observed for the films from the high-$Zn^{2+}$ solution. However, the intensities of the superlattice peaks in the $\beta'$-brass are expected to be significantly weaker than those of the fundamental peaks because the atomic scattering factors of Cu and Zn are close to each other [17, 18]. All the electrodeposited films are nevertheless the $\beta'$-brass, and the difference in the superlattice peak intensities is due to the difference in the preferred orientation of the lattice; the alloy films from the low-$Zn^{2+}$ solutions had a strong preferred orientation to the (111) facet, while that from the high-$Zn^{2+}$ solution had a (110) orientation.

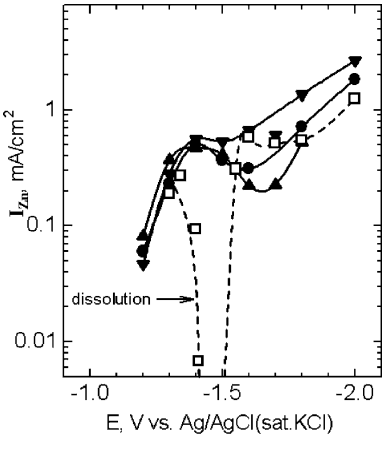


**Fig. 2** Partial *I–E* curves of Zn deposition in cyanide solutions. Solution compositions: *up triangles*: 0.30 M CuCN, 0.05 M $Zn(CN)_2$, 0.90 M NaCN; *circles*: 0.30 M CuCN, 0.10 M $Zn(CN)_2$, 1.00 M NaCN; *down triangles*: 0.30 M CuCN, 0.30 M $Zn(CN)_2$, 1.40 M NaCN; *squares*: 0.100 M $Zn(CN)_2$, 0.237 M NaCN

### *Mechanisms of the single-phase β′-brass deposition*

The single-phase $\beta'$-brass was deposited at −1.4 V, which corresponds to the high overpotential for Cu deposition and to the UPD region for Zn deposition; the separate deposition of Cu and that of Zn began at −0.94 V and −1.5 V, respectively. Cu electrodeposition at high overpotentials includes at least the following processes: (1) discharge of $Cu^{+}$–cyanide complex ions at the cathode surface, (2) coalescence of the discharged Cu atoms to form Cu nuclei, and (3) growth of the nuclei. The deposition of the single-phase $\beta'$-brass containing Cu at −1.4 V means that the crystal formation or growth of Cu or the solid solution of Zn in Cu did not occur at high overpotential for Cu, although the discharge of $Cu^{+}$ actually occurred. This suggests that the processes (2) and (3) were hindered by the UPD of Zn atoms onto the discharged Cu atoms; the UPD occurs immediately after the discharge of $Cu^{+}$ and before the coalescence of the discharged Cu atoms. The UPD of Zn and the formation of CuZn occur accumulatively as the discharge of the $Cu^{+}$–cyanide complex ions proceeds. Thus the accumulative UPD of Zn onto the discharged Cu atoms and the growth of the $\beta'$-brass nuclei result in the bulk electrodeposition of the single-phase $\beta'$-brass films. These mechanisms are summarized in Eqs. 1 and 2:

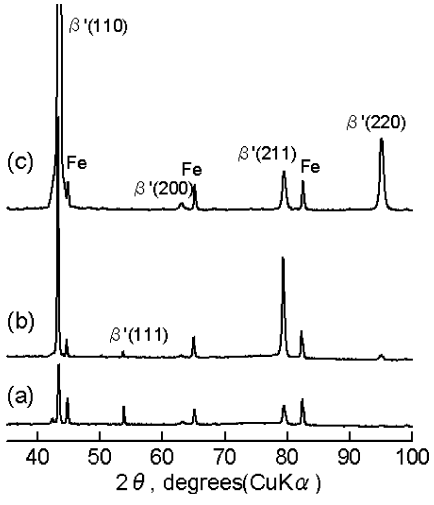


**Fig. 3** X-ray diffraction patterns of the electrodeposited Cu-Zn alloy films obtained at −1.4 V: (*a*) film obtained from 0.30 M CuCN, 0.05 M $Zn(CN)_2$, 0.90 M NaCN solution; (*b*) film obtained from 0.30 M CuCN, 0.10 M $Zn(CN)_2$, 1.00 M NaCN solution; (*c*) film obtained from 0.30 M CuCN, 0.30 M $Zn(CN)_2$, 1.40 M NaCN solution. "Fe" represents the diffraction peaks assigned to the Fe substrate

$$\mathrm{Cu(CN)}_n^{(n-1)-} + \mathrm{e}^- \rightarrow \mathrm{Cu} + n\mathrm{CN}^- \qquad n = 3,\ 4 \tag{1}$$

$$\mathrm{Zn(CN)}_4^{2-} + \mathrm{Cu} + 2\mathrm{e}^- \rightarrow \mathrm{CuZn} + 4\mathrm{CN}^- \tag{2}$$

Alloy film formation by UPD and subsequent "vertical" solid-state diffusion: contact immersion deposition of Sn onto Cu and Cu-Sn intermetallic phase layer growth

A kind of contact immersion metal film deposition was described by Summerlin and Ealy [19] and was named "the Alchemists' Dream Process". This process involves the electroless deposition of Zn onto a Cu substrate in an alkaline solution with suspended metallic Zn powder, which is partly dissolved as the zincate ion and partly remains as a suspension. Recently, it was shown that Zn deposition also occurs from the alkaline zincate solutions without the suspended Zn powder by contacting the substrate with a Zn sheet in the same solution [20, 21]. We showed that Zn is deposited in the UPD region and that the deposited Zn formed Cu-Zn intermetallic phases [22].

We also [23] found that Sn is deposited onto Cu from Sn(II)–citrate solutions via this type of the contact immersion process. The kinetics and the mechanisms of the Sn deposition and the composition and structure of the deposited films are shown here.

*Sn deposition kinetics and structural characterization of the deposited phases*

Scanning electron microscopy/energy dispersive X-ray (SEM/EDX) analysis confirmed the Sn deposition onto a Cu substrate in two kinds of contact immersion experiments. Figure 4 shows the amount of the deposited Sn as a function of the square root of the immersion time, $t^{1/2}$. The linear relationship between the deposited Sn and $t^{1/2}$ was clearly observed, showing that the kinetics of the film growth follow a parabolic rate law. In contrast, the weight of the contacted Sn decreased as the Sn film deposition onto Cu proceeded. The dissolution of the bulk Sn is the electron source for the deposition of the Sn films.

Figure 5 shows the change in the immersion potentials of Cu and Sn in the Sn(II)–citrate solution caused by short-circuiting. The immersion potential of Cu, $E_{\mathrm{Cu}}$, was about 400 mV positive to that of Sn. $E_{\mathrm{Cu}}$ was rapidly changed to the negative direction by short-circuiting, and a stable mixed potential, several millivolts positive to the immersion potential of Sn, was established in approximately 10 s. This potential change shows that the deposition of Sn occurred in the UPD region where the bulk Sn was dissolved. The dissolution of Sn controlled the mixed potential at which the UPD of Sn onto Cu is possible.

Figure 6 shows the XRD patterns of the deposited films. The major constituent of the films was $Cu_6Sn_5$ (JCPDS-ICDD, 02-0713). Weak extra peaks attributable to a metastable phase, $Cu_{10}Sn_3$ (JCPDS-ICDD, 26-0564), were observed in all samples. $Cu_3Sn$ (JCPDS-

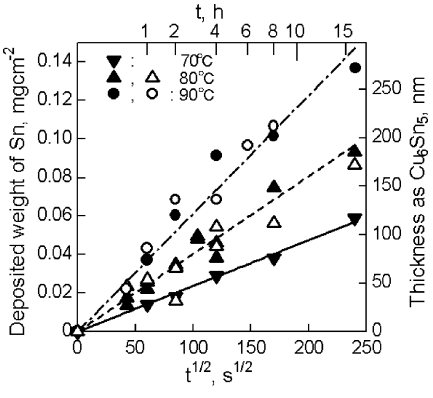


**Fig. 4** Weight of the deposited Sn in contact immersion deposition processes as a function of the square root of the immersion time, $t^{1/2}$. Solution composition: 0.1 M $SnSO_4$, 1.0 M trisodium citrate. *Open plots*: Cu sheet dipped in a solution with suspended Sn powder; *solid plots*: short-circuited immersion in a solution without suspended Sn powder; *down triangles*: 70 °C; *up triangles*: 80 °C; *circles*: 90 °C

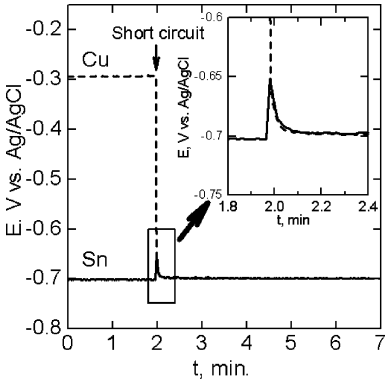


**Fig. 5** Change in the immersion potentials of Cu and Sn in the Sn(II)–citrate solution caused by a short-circuit

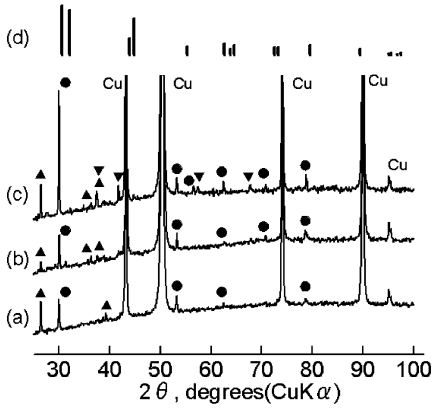


**Fig. 6** X-ray diffraction patterns of the Sn-deposited Cu substrate after short-circuited immersion for 16 h: (*a*) 70 °C, (*b*) 80 °C, (*c*) 90 °C, (*d*) peak position of $\beta$-Sn (JCPDS-ICDD, file 4-673). *Circles*: $Cu_6Sn_5$ (JCPDS-ICDD, file 2-0713); *up triangles*; $Cu_{10}Sn_3$ (JCPDS-ICDD, file 26-0564); *down triangles*: $Cu_3Sn$ (JCPDS-ICDD, file 1-1240)

ICDD, 01-1240) was also observed in the film at 90 °C. Nevertheless, the separate deposition of elemental Sn ($\beta$-Sn, JCPDS-ICDD, 04-0673) was not observed.

*Mechanisms of Cu-Sn alloy layer growth*

The formation and growth of the deposited metal–substrate metal alloys in the UPD region have been observed in several systems [7, 24, 25]. For example, Bort et al. [7] reported that a Ag-Cd alloy layer was grown onto Ag in a $CdSO_4$ solution in the UPD region up to 50 mV. They found that its growth followed a parabolic rate law, and derived the parabolic rate law theoretically, assuming solid-state diffusion through the alloy layer and a reversible (very fast) UPD at the surface. The parabolic rate law generally indicates the diffusion-controlled growth of the film and is presented by the equation:

$$\Delta x = \sqrt{2Dt} \tag{3}$$

where $\Delta x$ is the film thickness at time $t$, and $D$ is the mutual diffusion coefficient of the constituent atoms through the film.

A UPD/vertical solid-state diffusion mechanism can be proposed for the growth of the Cu-Sn alloy layer by contact immersion deposition, similar to those discussed by Budevski et al. [6] for the UPD of Cd on Ag. (1) A monoatomic Sn layer is formed at the Cu surface at potentials controlled in the UPD region by the bulk Sn dissolution; (2) a site exchange between the underpotentially deposited Sn atoms and the Cu substrate atoms supplies Cu atoms at the surface; (3) this also forms the nuclei of the Cu-Sn intermetallic phases; (4) the successive UPD of Sn onto Cu atoms occurs at the surface of the Cu-Sn intermetallic phase layer. The growth rate of the Cu-Sn intermetallic phase layer is limited by the mutual diffusion of Sn and Cu through the alloy layer.

The mutual diffusion coefficient, $D$, was estimated from the slope of the lines in Fig. 4 to be $1.12\times 10^{-15}$ cm$^2$ s$^{-1}$ at 70 °C, $3.22\times10^{-15}$ cm$^2$ s$^{-1}$ at 80 °C and $7.41\times10^{-15}$ cm$^2$ s$^{-1}$ at 90 °C. The activation energy of diffusion was determined to be 98.1 kJ mol$^{-1}$ K$^{-1}$ from the slope of the Arrhenius plots of $D$. This value agreed well with that of the diffusion-controlled growth of the $Cu_3Sn$ layer at the $Cu/Cu_6Sn_5$ interface, 95.5 kJ mol$^{-1}$ K$^{-1}$ [26], which is, to the authors' knowledge, the only value reported for diffusion through the Cu-Sn intermetallic phase. This agreement strongly suggests solid-state diffusion-controlled growth of the Cu-Sn intermetallic phase layers.

Intermetallic phase formation between electrodeposited metal and occluded metal nanoparticles: $Ag_3Sn$ phase formation in the Sn/Ag-nanoparticle composite plating

We recently reported [27, 28] that Sn-Ag alloy films were electrodeposited via "composite plating" from suspensions of Ag nanoparticles, which were formed spontaneously in the solutions containing $SnSO_4$, $K_4P_2O_7$ and $AgNO_3$.

*Ag nanoparticle suspensions for Sn-Ag alloy deposition*

The colored constituents of the black solution did not pass through the cellulose tube in the dialysis experiments. After 24-h dipping of a cellulose tube containing the black solution in water, Ag was not detected in the water outside the tube by ICP-AES measurements, but the Sn concentration was fully equilibrated inside and outside the tube. The colored constituents of the black solution were therefore polymers and/or solid particles larger than 2.4 nm containing Ag.

The dialysis was continued for 48 h, with frequent changes of the water outside the tube, in order to remove the small molecules and ions entirely from the tube. The SEM/EDX analysis of the residue in the tube showed that the major constituent was Ag, while Sn was not detected. Figure 7 shows the TEM image of the dialysis residue and the corresponding electron diffraction pattern. The dialysis residue was nanoparticles with diameters ranging from several nanometers to 10 nm. All the electron diffraction rings were assigned to the metallic (elemental) Ag. The existence of Ag nanoparticles in the solution was also confirmed from the UV-visible spectra showing a surface plasmon resonance peak at around 420 nm [29, 30]. Metallic Ag nanoparticles were probably formed via a fast redox reaction between $Sn^{2+}$ and $Ag^+$ ions.

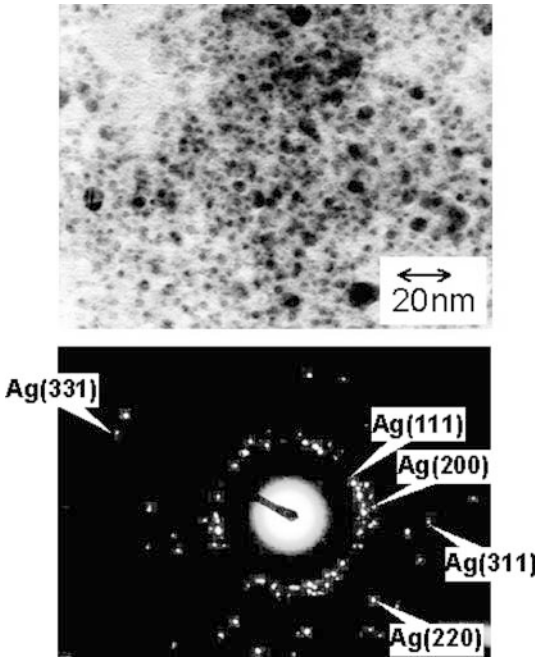


**Fig. 7** TEM image and the corresponding electron diffraction pattern of the dialysis residue of the Sn-Ag alloy deposition solution, showing Ag nanoparticles

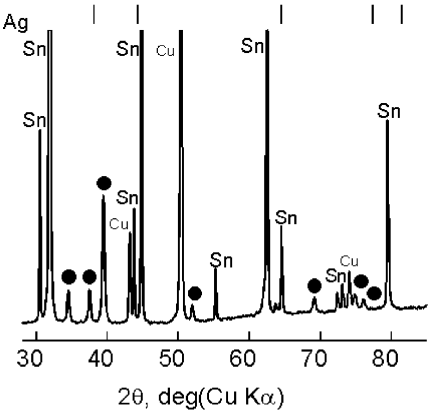


**Fig. 8** X-ray diffraction patterns of the Sn-Ag alloy film electrodeposited from the suspensions of Ag nanoparticles in $Sn^{2+}$–pyrophosphate complex ion solutions. *Circles*: $Ag_3Sn$; *Sn*: $\beta$-Sn; *Cu*: Cu substrate; *Ag*: peak position of Ag (JCPDS-ICDD, file 4-783)

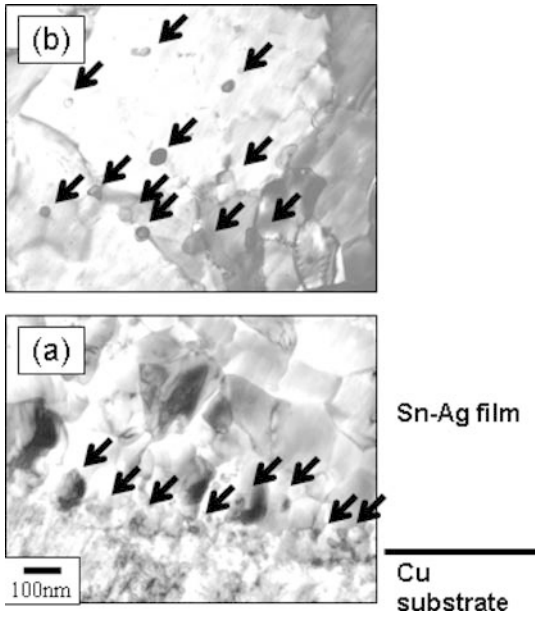


**Fig. 9** Cross-sectional TEM images of the electrodeposited Sn-Ag alloy film onto Cu: (**a**) Cu substrate interface; (**b**) near growing surface; *arrows* indicate the $Ag_3Sn$ particles

These results show that the black solutions are Ag nanoparticle suspensions in the $Sn^{2+}$–pyrophosphate complex ion solutions. We used these suspensions as the Sn/Ag-nanoparticle composite plating solutions.

### *Structural characterization of electrodeposited Sn-Ag alloy films*

Ag was actually codeposited with Sn from the $Sn^{2+}$–pyrophosphate/Ag-nanoparticle solution. Poly(ethylene glycol) was needed to obtain dense alloy films. As reported elsewhere [28, 31], the Ag contents of the electrodeposited films were almost constant at around 4 mass% over a wide current density range.

Figure 8 shows the XRD pattern of the deposited film. The XRD peaks were assigned to $\beta$-Sn (JCPDS-ICDD, 4-673) and the intermetallic compound $Ag_3Sn$ (JCPDS-ICDD, 4-800). The composite plating of Ag nanoparticles in the Sn matrix essentially involves the electrodeposited films containing elemental Ag particles dispersed in a Sn matrix. Nevertheless, the elemental Ag disappeared and $Ag_3Sn$ was formed without annealing. The deposited phases are identical with those expected from the equilibrium phase diagram [32].

Figure 9 shows the cross-sectional TEM images of the electrodeposited Sn-Ag alloy films onto Cu. The $\beta$-Sn grains were clearly observed, of which the sizes were around 100 nm near the substrate interface and around 1 μm in the bulk of the films. Fine $Ag_3Sn$ particles were randomly dispersed inside the $\beta$-Sn grains, along the grain boundaries, and at the substrate interface. The $\beta$-Sn grains and $Ag_3Sn$ particles were confirmed by selected area electron diffraction measurements (Nagao T, Fujiwara Y, Hoshika H, 2002, unpublished data). The microstructure of the deposited film is somewhat different from that of the thermally prepared Sn-3.5 mass% Ag eutectic alloys, where 1-μm long $Ag_3Sn$ fibers are not dispersed randomly but form a network for which the size is around 10 μm in a large $\beta$-Sn matrix [33].

The high electrical conductivity and the very small size of the occluded particles, Ag, can account for the disappearance of the elemental Ag and the formation of $Ag_3Sn$ in the deposited films. Sn can be deposited onto the conductive Ag particles adsorbed on the cathode. In addition, site exchange between deposited Sn atoms and the Ag "substrate" atoms occurs across a certain number of atomic layers due to a strong Sn-Ag interaction [6]. The Sn-Ag interaction is suggested based on the non-zero solubility of Sn in Ag and the existence of the stable intermetallic phases. The Ag particles are so small that the site exchange extends into the whole particles, resulting in the disappearance of Ag and the formation of $Ag_3Sn$ in the deposits.

## Conclusions

Three cases of electrochemical deposition of intermetallic phases were exemplified and the deposition mechanisms were discussed.

1. The Cu-Zn alloy films composed of a single-phase $\beta'$-brass superlattice were electrodeposited from cyanide solutions at underpotentials of Zn. An accumulative UPD mechanism was proposed for the single-phase $\beta'$-brass deposition. The UPD of Zn atoms onto the discharged Cu atoms inhibits the nucleation and growth of Cu and occurs accumulatively as the Cu discharge proceeds. This leads to bulk deposition of the single-phase $\beta'$-brass films.

2. The Cu-Sn intermetallic phases were formed by contact immersion deposition of Sn onto Cu. A UPD/vertical solid-state diffusion mechanism was proposed for the intermetallic phase layer growth. The site exchange between the underpotentially deposited Sn atoms and the substrate Cu atoms provides Cu atoms to the surface, on which the Sn UPD occurs successively. The bulk intermetallic phase layer is thus formed, and its growth rate is limited by the vertical solid-state diffusion through the layer.
3. Sn-Ag alloy films were electrodeposited from suspensions of Ag nanoparticles in the $Sn^{2+}$–pyrophosphate complex ion solutions via composite plating. The deposited films did not contain elemental Ag but were composed of $\beta$-Sn and $Ag_3Sn$. The atomic site exchange at the interface between the Sn matrix and the occluded Ag nanoparticles can account for the disappearance of elemental Ag and the formation of the intermetallic phase $Ag_3Sn$. The occluded Ag particles are so small that the site exchange extends into the whole particles.

The first two examples are cases where the UPD of the less noble alloy component is essential to the deposition of the intermetallic phases. In contrast, the role of the atomic site exchange at the interface between the different phases was illustrated in the second and the third examples; the second example showed the role of the site exchange between the underpotentially deposited Sn and the Cu substrate, and the third showed that at the Sn matrix/occluded Ag-nanoparticle interface inside the deposited alloy films or at the growing surface.

Further studies concerning the nanometer-scale structure and the dynamics of the growing surface are needed to confirm the proposed mechanisms completely and hence to gain deeper insight into the electrochemical deposition of the intermetallic phases. These results will shed light on the electrochemical deposition of the tailored-structure alloy films.

## References


1. Brenner A (1963) Electrodeposition of alloys. Academic Press, New York
2. Augis JA, Bennett JE (1978) J Electrochem Soc 125:335
3. Omi T, Kokunai S, Yamamoto H (1976) Trans Jpn Inst Met 17:370
4. Panicker MPR, Knaster M, Kroger FA (1978) J Electrochem Soc 125:566
5. Murase K, Uchida H, Hirato T, Awakura Y (1978) J Electrochem Soc 146:531
6. Budevski E, Stoikov G, Lorentz WJ (1996) Electrochemical phase formation and growth, VCH, Weinheim, pp 128–146
7. Bort H, Juttner K, Lorentz WJ, Stoikov G (1983) Electrochim Acta 28:993
8. Horkans J, Hsu Chang I, Andricacos PC, Deligianni H (1995) J Electrochem Soc 142:2244
9. Safranek WH (1990) Plat Surf Finish 77(2):12
10. Kowalski AJ (1998) Plat Surf Finish 85(11):36
11. Zhang Y, Abys JA (2000) Tin and tin alloys for lead-free solder. In: Schlesinger M, Paunovic M (eds) Modern electroplating, 4th edn. Wiley, New York, pp 241–287
12. Brenner A (1963) Electrodeposition of alloys, vol 1. Academic Press, New York, pp 411–496
13. Smith RM, Martell AE (1976) Critical stability constants, vol 4. Plenum Press, London, p 26
14. Fujiwara Y, Enomoto H (2000) J Electrochem Soc 147:1840
15. Hansen M, Anderko K (1958) Constitution of binary alloys. McGraw-Hill, New York, pp 649–655
16. Kittel C (1996) Introduction to solid state physics, 7th edn. Wiley, New York, pp 617–621
17. Cullity BD (1978) Elements of X-ray diffraction, 2nd edn. Addison-Wesley, Reading, Mass
18. Maslen EN, Fox AG, O'Keef MA (1992) In: Wilson ALC (ed) International tables for crystallography, vol C. Kluwer, Dordrecht, p 475
19. Summerlin LR, Ealy JL (1988) Chemical demonstrations. American Chemical Society, Washington
20. Tsuchiya T (1996) Memoirs Joto High School (Tokyo) 14:47
21. Takahashi T, Matsui H, Matsuda S, Yoshida Y, Aono T, Takashima Y (1996) Memoirs Joto High School (Tokyo) 14:49
22. Fujiwara Y, Enomoto H, Yoshikawa J, Yamauchi E (2001) Hyomen Gijutsu (J Surf Finish Soc Jpn) 52:141
23. Fujiwara Y (2003) Thin Solid Films 425:121
24. Schmidt E, Christen H, Bleyeler P (1973) J Electroanal Chem 42:275
25. Vidu R, Hara S (2000) Surf Sci 452:229
26. Tu KN, Thompson RD (192) Acta Metall 30:947
27. Fujiwara Y, Yarimizu Y, Enomoto H, Narahara T, Funada K (1999) Hyomen Gijutsu (J Surf Finish Soc Jpn) 50:1173
28. Fujiwara Y, Yarimizu Y, Enomoto H, Narahara T, Funada K (2000) Proc 3rd international symposium on electrochemical technology applications in electronics. (Proceedings series PV 99-34) The Electrochemical Society, Pennington, NJ, p 363
29. Fujiwara Y, Enomoto H, Nagao T, Hoshika H (2003) Surf Coat Technol 169:100
30. Novak JP, Feldheim DL (2000) J Am Chem Soc 122:3979
31. Fujiwara Y, Nagao T, Enomoto H, Hoshika H (2002) J Jpn Inst Electron Packag 5:366
32. Hansen M, Anderko K (1958) Constitution of binary alloys. McGraw-Hill, New York, pp 52–54
33. Suganuma K, Huk S, Kim K, Nakase H, Nakamura Y (2001) Mater Trans Jpn Inst Met 42:286